Graphene based Van der Waals contacts on MoS_2 field effect transistors

Vivek Mootheri[1,2], Goutham Arutchelvan[1], Sreetama Banerjee[1], Surajit Sutar[1], Alessandra Leonhardt[1,3], Marie-Emmanuelle Boulon[1], Cedric Huyghebaert[1], Michel Houssa[4], Inge Asselberghs[1], Iuliana Radu[1], Marc Heyns[1,2] and Dennis Lin[1]

[1] IMEC, Kapeldreef 75, Leuven, Belgium,
[2] Department of Materials Engineering, KU Leuven, Belgium,
[3] Department of Chemistry, KU Leuven, Belgium,
[4] Department of Physics and Astronomy, KU Leuven, Belgium

Abstract

Device performance of two dimensional (2D) material based field effect transistors is severely limited by the relatively high contact resistance encountered at the contact-channel interface. Metal-graphene hybrid contacts have been previously used to improve the contact resistance of devices based on thick exfoliated materials. Here we report a novel 2D FET fabrication process entailing the transfer of metal-graphene hybrid contacts on top of 3 monolayer-thick chemical vapor deposition (CVD) MoS_2, enabling a lithography free contacting strategy, with respect to MoS_2. Three different metal-graphene stacks consisting of Ni, Pd and Ru, have been fabricated, transferred onto MoS_2 and characterized extensively using electrical and physical characterization techniques. We find strong correlation between the measured electrical characteristics and physical characterization of the contact interface. From Raman spectra measurement, maximum charge transfer of 1.7×10^{13} cm^{-2} is observed between graphene and Ru, leading to an improved contact resistance for MoS_2devices with Ru-Gr contacts. Ru-Gr contact shows the lowest contact resistance of 9.34 kΩ μm among the three metal-graphene contact stacks reported in this article. This contact resistance is also the best among reported CVD grown graphene contacted MoS_2 devices. Using more than 400 devices, we study the impact of the different metal-graphene contacts on other electrical parameters such as hysteresis, sub-threshold swing and threshold voltage. The metal-graphene contact stack transfer technique represents a technologically relevant contacting approach which can be further up-scaled to larger wafer areas.

1. Introduction

Two dimensional (2D) materials have attracted great attention as potential alternatives to silicon in future complementary metal-oxide-semiconductor (CMOS) technology nodes [1–3]. Among the various 2D transition metal dichalcogenides (TMDCs), one of the most promising and most researched for use in high performance logic devices is molybdenum disulfide (MoS_2). MoS_2 field effect transistors (FETs) have been utilized in several applications ranging from gas sensors [4] to photodetectors [5], owing to good gate control and high sensitivity to the ambient conditions in these devices. However, device performance of MoS_2 FETs is severely limited by the relatively high contact resistance encountered, caused by the formation of a schottky barrier (SB) at the interface between the metal and the 2D channel [6]. In conventional CMOS technology, ohmic contacts are formed by substitution/impurity doping of the source and drain region with electron/hole dopants for NMOS and PMOS respectively. In the case of ultrathin MoS_2 FETs, use of conventional doping techniques can result in damage to the MoS_2 layer. There are several strategies suggested to reduce the contact resistance like surface doping [7–9], ultra high vacuum metal deposition [10], phase engineered contacts [11] and one dimensional edge contacts [12]. Although all these methods claim to improve device characteristics, in reality, there are multiple drawbacks with each of these approaches which impede the use of these techniques in technologically relevant device architectures. For instance, although surface doping strategies increases the ON current, they significantly degrade the OFF state [13]. Similarly, lithium intercalated '1 T' MoS_2 is a metastable 'metallic' state which can relax back to a more stable '2 H' semiconducting state in a short span of time or upon temperature treatments [14].

On the other hand, an emerging contact improvement concept is the use of graphene as an interlayer contact to MoS_2 FETs, due to graphene's semi-metallic nature [15, 16]. Studies have shown that the work function of graphene can be lowered by adsorption of metals on top of it [16, 17]. When graphene is chemisorped on a metal substrate, a charge transfer between the two materials result in doping of the graphene layer, thereby causing work function reduction of the whole stack. This leads to a lower Schottky barrier when the metal-graphene stack is used to contact a TMDC layer. Graphene also provides an atomically sharp interface without dangling bonds that is expected to prevent the Fermi Level pinning occurring at the contact interface. As a result of these reasons there has been widespread interest in developing graphene contacts to TMDC FETs [18, 19]. However, most of the aforementioned works were flake TMDC devices, obtained from exfoliation, to form stacked Van der Waals (VdW) heterostructures. Thus there is no precise control on the thickness of MoS_2 or graphene. These factors play a critical role in estimating the device performance [20]. Furthermore, a device made using flakes cannot be used as a prototype for a device based on large area material due to observed morphological differences between the two types, ranging from the presence of grain boundaries to differences in defect density.

In this work, we fabricate MoS_2 FETs with metal-graphene hybrid top contacts. The 2D materials constituting the channel and contact of the fabricated devices have been synthesized using chemical vapor deposition (CVD) with precise control of thickness over large areas. A novel 2D FET fabrication process is developed to transfer metal-graphene hybrid contacts on top of the CVD MoS_2. This process enables us to contact MoS_2 in a '*lithography free, self-aligned*' approach: no lithography is done on MoS_2 for defining the contacts while the graphene and metal layers of the contact stack are aligned to each other. Over 400 devices spread out in 30 repeating transmission line measurement (TLM) structures have been electrically measured and analyzed to extract and compare statistically relevant trends in transistor and contact parameters. We fabricate Ru-Gr top contacts on MoS_2 for the first time and observe the least contact resistance among the metal-graphene stacks studied. The unique contact transfer method presented in this article has exhibited reproducible results over several attempts and represents a technologically relevant technique which can be further up-scaled to larger wafer areas.

2. Methods

MoS_2 was grown using metal-organic chemical vapor deposition (MOCVD) on a sapphire template wafer. Sapphire template wafer was chosen since it was shown to have epitaxial growth [21] for MoS_2 layers. Epitaxial alignment ensures that the concentration of grain boundaries is lower compared to growing on an amorphous substrate like SiO_2 [22]. Rutherford Backscattering Spectrometry confirms that the average thickness is 3.7 layers, implying three closed monolayers and islands of fourth layer on top. The MoS_2 layer was then transferred onto 50 nm thermally grown SiO_2/p^{++} Si substrate. The details of the transfer and cleaning process are described in the supplementary information section S1. In order to understand changes in electrical characteristics solely due to the contact interface and discount any variation in MoS_2 growth quality or processing, CVD-grown MoS_2 for all samples are taken from single growth and processing conditions are kept identical.

For the fabrication of contacts, we grow single layer graphene (SLG) on Pt foil in a vertical cold-wall AIXTRON Black Magic Pro 6" CVD system [23]. Graphene was transferred to a 50 nm thermally grown SiO_2/p^{++} Si substrate using water based delamination process [24]. To clean the transfer polymer residue, the sample is annealed in 5% forming gas for 1 h at 350 °C. Contacts were fabricated on this SLG sample using conventional electron beam lithography, with a minimum feature size of 500 nm. After development, three different metal stacks were deposited on the graphene layer of each sample at a base pressure of 5.5×10^{-7} mbar using an electron gun evaporation system (Pfeiffer E-Gun PLS 580) at a rate of 0.8–0.9 Å/s. During the deposition the sample is kept at a constant temperature of 16 °C. The first metal stack consists of 10 nm Ni and a capping layer of 20 nm Pd. Second metal stack consists of 30 nm Pd and the third one includes 10 nm Ru and 20 nm Pd as capping layer. The metal was then lifted-off forming contacts on top of graphene. To isolate the graphene in between the contact pads, the sample was exposed to a soft oxygen plasma etch (100 W, 45 s). Thus, graphene/metal pillars were formed.
To form a VdW contact with MoS_2, these contact pillars were transferred onto MoS_2. This novel transfer process includes using the difference in surface energy between graphene and SiO_2, similar to the process of transfer of MoS_2 from sapphire growth template wafer to SiO_2 susbtrate. A 395 nm thick layer of PMMA was spin-coated onto the sample which contains graphene/metal pillars. A thermal release tape (TRT) was then attached to the PMMA layer to provide additional support. This was then immersed into a beaker containing deionized water at 80 °C kept in an ultrasonic bath. Since graphene is hydrophobic and SiO_2 hydrophilic, the water molecules intercalated between the two layers and released the metal-graphene stack from the SiO_2 substrate. After 6 min, slowly peeling out the TRT, released the SLG/metal pillars from the SiO_2 substrate onto the PMMA layer supported on TRT. The entire contact pillar set was removed with a yield over 95% , reproducible over several trials on all the metal stacks. The contact stack/PMMA/TRT heterostack was then laminated onto cleaned MoS_2 surface at 80 °C. Subsequently, TRT tape is removed and PMMA is dissolved in hot acetone at 50 °C. The three different metal-graphene stacks after being laminated onto MoS_2, were annealed (200 °C for 8 h at 10^{-6} mbar) and electrically characterized in a N_2ambient with a PA300 semiautomatic probe station and B1500A parameter analyzer. On each sample, 30 device sets were measured and each set consisted of 15 different channel lengths varying from 500 nm to 20 μm. The process flow for the transfer of contacts is depicted in figure 1. The aforementioned process enable us to reliably fabricate and transfer contacts onto CVD MoS_2without any processing on the layer, avoiding the damage that is expected when direct processing is carried out on the MoS_2 layer [25, 26]. However, it is important to note that removal of the very thin (1–3 nm) PMMA residue layer (formed from MoS_2 transfer step) is critical in improving the device characteristics. Failure to remove the PMMA layer would result in polymer residue between the contact stack and the MoS_2 channel, which would degrade the contact resistance.

3. Results and discussion

Ru, Ni and Pd have been chosen as contact metals for this study due to three main reasons. Firstly, since the aim of the experiment is to reduce the overall contact resistance, it is vital to reduce the contact resistance at the metal-graphene interface, in addition to the graphene-MoS_2 interface. Previous reports have shown that these three metals have a high degree of hybridization and low contact resistance with graphene [17, 27]. Secondly, these particular metals have lesser metal-graphene separation and high degree of hybridization, which results in good adhesion between the two layers. During the water intercalation based contact transfer process, if the metal does not adhere well to the graphene layer, the pads would delaminate without graphene on them. Therefore, strong adhesion between graphene and metal helps in the water delamination process, enabling the transfer of the metal-graphene contact stack. Lastly, Ru-Gr has been theoretically shown to reduce the Schottky barrier height (SBH) by interfacial charge transfer [28] and this study aims to experimentally prove this mechanism.
The study involves two different interfaces, the metal-graphene interface which is characterized using Raman spectroscopy and kelvin force probe microscopy (KPFM) and the contact stack-MoS_2interface characterized using electrical measurements. The results are divided into these two sections.

3.1. Physical characterization

The process of transferring metal-graphene contact stacks allows us to inspect the contact interface after delamination of the contact pads from the SiO_2 substrate. The TRT/PMMA stamp onto which the metal pads delaminate can be inverted to investigate the presence of graphene. Raman spectroscopy has been utilized to detect and characterize the graphene on top of the metal pads (inverted configuration) and analyze doping of the graphene film. A Raman spectra mapping was conducted on an area of $10 \times 10\ \mu m^2$ for each inverted SLG/metal stack, using a 532 nm laser at a power density of 1.1 mW μm^{-2}. A

schematic of the Raman spectra acquisition procedure and the median Raman spectra for the Ru-Gr and Pd-Gr contact stacks are shown in figures 2(a) and (b), respectively. When Raman spectroscopy was conducted on the Ni-Gr stack, the obtained Raman signal matched perfectly with the spectra obtained from the PMMA/TRT background, especially in the region from 1550 to 1750 cm^{-1} (figure 2(c)). The strong chemical interaction between graphene and Ni(111) changes graphene's p_z orbital energy resulting in the loss of graphene's Raman signal [17]. It is important to note that, in this study, graphene on Ru shows a strongly suppressed Raman signal which can be attributed to Ru having an amorphous structure when deposited on graphene [17]. Although this could be the case for Ni-Gr stack as well, we see a strong contribution in the Raman spectra from the background in this stack, which is not present in the Ru-Gr stack. This strong influence from the background spectra could be due to a more *templated* deposition of Ni(111) on graphene due to low lattice mismatch of this phase with graphene [17]. Thus we believe that there is a strong hybridization in the case of Ni-Gr and graphene no longer has its electronic band structure preserved on Ni.

To further understand the nature of the metal-graphene stack, the frequency of the 2D peak is plotted with the corresponding G peak frequency, as shown in figure 2(d). The graph also presents calculations to deduce uniaxial native strain and charge doping from the peak positions, following the methodology detailed in previous reports [29]. The two axes shown in the picture depicts the doping axis and strain axis, respectively, and each line parallel to the strain (doping) axis depicts a particular value of doping (strain). For Ru-Gr which has a split G-peak, the arithmetic mean of the individual peak's frequency is used as the G peak frequency value. From the analysis it can be discerned that graphene is more doped on Ru than on Pd. The average value of doping is about 1.7×10^{13} cm^{-2} for the Ru-Gr stack while it is about 7×10^{12} cm^{-2} for the Pd-Gr stack. Both stacks are tensile strained with a median value of about 0.3% for Pd-Gr and 0.7% for Ru-Gr. From DFT studies [16, 28], it has been found that when graphene is chemisorbed on Ni and Ru, the work function of the heterostructure electrode becomes 3.64 and 3.47 eV, respectively. This would result in these contact stacks transferring charge to MoS_2 (electron affinity of 4.3 eV) when they come in contact.

KPFM measurements were conducted on the metal-graphene stacks to verify the aforementioned hypothesis of work function reduction upon graphene adsorption on metal. The measurements were done in BRUKER *Dimension One* AFM mounted in an argon glove box. The variation in topography and contact potential difference (CPD) for each contact stack is depicted in figure 3. We observe that the surface roughness is least for the Pd-Gr (RMS roughness of 0.9 nm) sample and most for the Ru-Gr sample (RMS roughness of 1.43 nm) with Ni-Gr in between (RMS roughness of 1.29 nm). The average CPD value calculated from the KPFM map of each contact stack is used to calculate the work function of the sample by using the relation $WF = eV_{CPD} + WF^{tip}$, where WF^{tip} is calibrated using a standard Au sample with a known work function of 4.95 eV. The average work function calculated for each stack is 4.33 4.7 and 4.91 eV for Ru-Gr, Pd-Gr and Ni-Gr respectively. This proves that graphene adsorption influences the work function of these electrodes due to the doping from the metal contacts. It is important to note that KPFM maps shown in figure 3 are obtained before annealing the contact stack. We observe a larger shift in the threshold voltage after annealing, for the Ru-Gr stack, indicating further reduction of work function of the contacts after annealing (see supplementary section S2). In the CPD map of Ni-Gr stack, we see regions of lower work function which correspond to higher topographical features. This could be a result of higher hybridization locally which reduces the work function in these regions. Although similar topographical features are seen in the Ru-Gr stack, we do not see significant variation of work function corresponding to these features. More experiments are required to analyze the chemical composition of these higher topographical features and understand the reasons for the observed local reduction of work function in the Ni-Gr stack. Nevertheless, from the KPFM mapping experiment we quantify the work function of each contact stack and observe that the work function is modulated when graphene is adsorbed on metal with the lowest work function measured for Ru-Gr contact stack.

3.2. Electrical characterization

Among the three different contact stacks, Ru-Gr stack has a higher ON current and more negative threshold voltage as observed from the median transfer characteristics shown in figure 4(b). When source-drain current at a fixed charge density of 1.5×10^{13} cm^{-2} is plotted against channel length, as shown in figure 4(c), we observe that Ru-Gr contacts inject 1.8 times higher median current than the Ni-Gr contacts, for the shortest channel length. This fixed charge density is calculated as $n_{2D} = (C_{ox}/q)(V_{GS} - V_T)$, where C_{ox} is the back gate capacitance and $V_{GS} - V_T$ represents the gate voltage overdrive. Negative threshold voltage and higher ON current for Ru-Gr stack is consistent with the theory of charge transfer from the metal to the graphene layer, which lowers the work function of the contact stack thereby

reducing the SBH at the source. Consequently, this turns on the FET at a lower gate voltage and injects higher current due to smaller SBH. The reduction in work function is more for the Ru-Gr stack compared to the Ni-Gr stack, thereby resulting in 1.8 times higher ON current at the same overdrive voltage.

We observe a strong correlation between the physical characterization of contact interface and the measured electrical trend. In contrast to Pd-Gr contact stack, Ni-Gr stack injects more current below channel length of 1.5 μm, as seen from the transistor current scaling behavior shown in figure 4(c). At these channel lengths, contact resistance is the dominant factor in total measured resistance, implying a lower contact resistance for the Ni-Gr contact stack. As seen from the KPFM mapping in figure 3, patches of lower work function are detected on the Ni-Gr stack while patches of higher work function are observed in the Pd-Gr stack. This elucidates why we measure an increase in ON current in the Ni-Gr stack compared to the Pd-Gr stack, for shorter channel lengths where contacts significantly determine the characteristics. Median ON current of Ni-Gr stack falls slightly below the values for Ru-Gr and Pd-Gr stack for the long channels ($LCH > 10\ \mu$m). We would like to note that this is an artifact of the larger spread observed in the case of Ni-Gr contact stack. This larger variability can be attributed to the frequent occurrence of islands of higher work function observed in the KPFM map of the Ni-Gr contact interface.

TLM measurements (figure 4(d)) are used to calculate the contact resistance of each of the metal-graphene stacks. The results are shown in figure 4(d) and (summarized) in table 1. The source drain resistance (R_{TOT}) at a fixed charge density of 1.5×10^{13} cm^{-2} was extracted for all the devices and plotted as a function of their respective channel length (L_{CH}). Abscissa intercept of the graph corresponds to twice the contact resistance and the slope gives the sheet resistance in the channel. Longer channels ($L_{CH} > 10\ \mu$m) are excluded from the fit since higher channel resistance of these devices can influence the linear fit more significantly than shorter channels. Furthermore, the fit was conducted by iteratively screening the outliers, fitting the remaining data points and ensuring the residuals of the fit are normally distributed. By eliminating the longer channels and conducting iterative screening, we ensure a reliable extraction of contact resistance.

Extracted contact resistance is least for Ru-Gr stack (9.34 ± 0.245 kΩ μm), followed by Ni-Gr stack (17.2 ± 1.33 kΩ μm) and highest for Pd-Gr stack (22.71 ± 0.529 kΩ μm). Charge transfer from the metal to the graphene layer results in work function reduction of the contact stack, lowering the SBH and reducing the contact resistance. This hypothesis is in agreement with the doping extracted from Raman mapping, where graphene on Ru is more doped compared to graphene on Pd. The contact resistance can be further improved by optimizing the contact transfer approach to fabricate FETs with ultra-scaled channel lengths. Sheet resistance calculated from the TLM fit is used to estimate the field effect mobility (μ) using the relation $\mu = (qn_{2D}R_{SH})^{-1}$. The calculated mobility values are of the same order of magnitude for all metal-graphene stacks, proving beyond doubt that processing conditions are similar among all cases. In contrast to Ru-Gr and Pd-Gr contact stacks, mobility value of Ni-Gr contact stack is slightly degraded. This degradation is an artifact of the larger variability found in the Ni-Gr contact stack caused by an irregular contact interface, as observed from the KPFM characterization.

Since the channel material was taken from the same growth and all samples were processed under identical conditions, it is reasonable to believe that variations in various transistor characteristics arise from the differences in the contact stack. In order to interpret these differences, we analyze trends in sub-threshold swing (SS), threshold voltage roll-off and hysteresis, as shown in figure 5.

Highest median SS is observed for Ru-Gr contacts while the lowest median SS is observed for Pd-Gr contacts, as shown in figure 5(a). Sub-threshold conduction in Schottky Barrier FETs (SB-FETs) is controlled by transport along the contact interface, which involves two dominant mechanisms: thermionic emission over the SB and tunneling through the SB. Therefore, OFF state in these SB-FETs is limited by gate control over the contact interface [30–32]. Two important parameters in this work that influence the SS are doping of the contact interface and the nature of the interaction between the metal and the graphene layer. When doping at the contact interface increases, gate control over the contact interface decreases, thereby degrading the OFF state and SS. Additionally, higher electron density at the contact interface would result in greater chemical interaction between MoS_2 and the contact stack, leading to bandgap states in MoS_2 which would cause a degraded OFF state. As inferred from the physical characterization section, doping at the contact interface is strongly correlated to the degree of hybridization between graphene and metal. Graphene on Ru is relatively more doped than graphene on Pd and Ni, resulting in poor gate control over the contact interface which leads to a degraded SS and OFF state. Raman characterization of the metal-graphene stack shows that graphene's Dirac cone is preserved on Pd. Graphene's pristine linear band dispersion ensures a relatively small density of high energy fermi-tail states compared to a normal metal [33]. This ensures a steeper turn on around flat band voltage as states become available for $V_{GS} > V_{FB}$.

The change of threshold voltage (calculated using the extrapolation in the linear region (ELR) method [34]) for each contact stack is shown in figure 5(b). The ELR method is used to extract threshold voltage since it gives the most accurate value of charge density in the linear regime of transistor operation. Threshold voltage of the 1 μm channel has a Gaussian distribution for all three contact stacks and $\sigma_{V_{th}}$ was found to be 1.79, 1.25 and 1.22 V for Ru-Gr, Ni-Gr and Pd-Gr respectively. These values correspond to a charge density variation of 7.70 × 10^{11} cm^{-2}, 5.39 × 10^{11} cm^{-2}, and 5.26 × 10^{11} cm^{-2}, which are an order of magnitude smaller compared to the predictions for 2 nm thick UTB SOI silicon FETs from body thickness variation alone [35]. A sharp decrease in threshold voltage was observed for the Ru-Gr contact stack, with the threshold voltage being entirely negative for the 1 μm channel. A significant negative threshold voltage arises from the work function reduction of the contact stack, due to graphene adsorption, which causes charge transfer between the contact and MoS_2. This is also reported in a DFT study of Ru-Gr contacts on MoS_2[28], where interface charge transfer is highest for Ru-Gr contacts.

Median hysteresis, shown in figure 5(c), falls in the same range (~2 V) for Ru-Gr and Pd-Gr contact stacks, with significantly low variation for short and long channels. However, we observe a large variation in the hysteresis of Ni-Gr contact stack for all channel lengths. Hysteresis is calculated as the difference in the gate voltage between the forward and backward sweep at a fixed current density of 10 nA μm^{-1}. Previous reports of hysteresis in MoS_2 FETs hypothesize traps in the MoS_2-SiO_2 interface as the main contributor [36, 37]. In this study, since all three substrates are cleaned in an identical approach, we interpret the differences found between Ni-Gr stack and Ru-Gr/Pd-Gr stack to be arising from contact interface difference. We speculate that the large spread in the case of Ni-Gr contacts could be caused by the smaller work function patches forming an irregular interface, as seen from the KPFM scan in figure 3. This would potentially result in interface states that could contribute to the observed hysteresis. Nevertheless, more experiments need to be carried out to prove this hypothesis and explain the large variability of hysteresis in Ni-Gr contact stack.

The variability found in SS and threshold voltage within the same channel length can be attributed to local variations in thickness of the MoS_2 channel (typical for CVD MoS_2) and differences in the metal-graphene contact stack. When the MoS_2 thickness changes, there is a local change in the characteristic length($\lambda = \sqrt{\frac{\epsilon_s t_s t_{ox}}{\epsilon_{ox}}}$ where $\epsilon_{ox} = 6.9 \times 10^{-8}$ F cm^{-2}, t_{ox} = 50 nm) [38], which is manifested as variability in both SS and threshold voltage. This is an intrinsic source of variability in all our samples. In addition to this, physical characterization of the contact interface revealed that higher the hybridization of graphene with metal, greater is the charge transfer between them, resulting in lower work function of the contact interface. Chemical interaction between metal and graphene leads to the destruction of graphene's linear band dispersion, forming a non-uniform contact interface with large variability in work function, as seen in the case of Ni-Gr. In contrast, graphene has relatively lesser hybridization with Pd leading to the formation of a uniform contact interface, reducing the measured variability of various transistor characteristics.

In figure 6, we have compiled a benchmark plot to compare our devices with previous reports of graphene contacted MoS_2 devices. Ru-Gr hetero-stack based MoS_2 devices, with a nominal channel thickness of 2.01 nm (3 layers), exhibit a contact resistance of 9.34 kΩ μm and presents the best case among CVD-grown devices. The contact resistance of previously reported devices were plotted as a function of the channel thickness, for both CVD-grown and flake (exfoliation) based devices. In previous reports of flake based devices, the semiconductor thickness was significantly high, resulting in higher ON current and lower contact resistance. In ultra-scaled devices (L_{CH} <100 nm), a thick channel would result in poor gate control and bad ON-OFF ratio. Thinner channels are technologically relevant due to better gate control and lesser impact of short channel effects. We would like to note that our fabrication methodology is simpler, compatible with CVD-grown material based processing and has a high yield of devices. The contact resistance is expected to further reduce by using short channel devices in combination with a scaled EOT oxide.

In conclusion, this study demonstrates a simple method of transferring metal-graphene hybrid contacts onto CVD MoS_2 enabling us to contact MoS_2 without any direct processing on the 2D layer. Ni-Gr, Pd-Gr and Ru-Gr contact stacks have been fabricated and transferred onto MOCVD grown MoS_2 using a novel contact transfer process. The reproducibility of the process has been confirmed by multiple transfers, all resulting in a high yield of devices. Raman spectroscopy confirms the presence of graphene after the contact transfer process and helps us to quantitatively describe the doping and/or strain induced on the graphene surface due to the metal deposition process. KPFM measurements confirm the reduction of work function of the contact stack when graphene is adsorbed on metal, with the smallest work function for the Ru-Gr stack. Detailed electrical characterization has been conducted on more than 400 fabricated devices, spread across each sample. Hysteresis, SS and threshold voltage roll-off have been electrically characterized and analyzed. Ru-Gr contact stack shows the lowest contact resistance of 9.34 kΩ μm

among the three metal-graphene stacks studied and also among reported graphene contacted CVD-grown MoS_2devices. The methodology of contact transfer paves way to easily characterize fast-degrading 2D materials by pre-fabricating contacts and transferring them at once onto the fast-degrading 2D material. This technique represents a technologically relevant contacting approach which can be further up-scaled to larger wafer areas leveraging on transfer equipment [47].

Acknowledgments

The authors would like to thank N A Pinna and R Verheyen for their excellent processing and insightful discussions. We would also like to thank J Serron, A Minj for the KPFM measurements, S Sergeant and S Achra for the Raman measurements and the Beyond CMOS program at IMEC for financial support.

References

[1] Radisavljevic B, Radenovic A, Brivio J, Giacometti V and Kis A 2011 *Nat. Nanotechnol.* **6** 147–50 0402594v3

[2] Das S, Chen H Y, Penumatcha A V and Appenzeller J 2013 *Nano Lett.* **13** 100–5

[3] Wang Q H, Kalantar-Zadeh K, Kis A, Coleman J N and Strano M S 2012 *Nat. Nanotechnol.* **7** 699

[4] Late D J *et al* 2013 *ACS Nano* **7** 4879–91

[5] Lopez-Sanchez O, Lembke D, Kayci M, Radenovic A and Kis A 2013 *Nat. Nanotechnol.* **8** 497

[6] Schulman D S, Arnold A J and Das S 2018 *Chem. Soc. Rev.* **47** 3037–58

[7] McDonnell S, Addou R, Buie C, Wallace R M and Hinkle C L 2014 *ACS Nano* **8** 2880–8

[8] Yang L *et al* 2014 *Nano Lett.* **14** 6275–80

[9] Lockhart De La Rosa C J *et al* 2016 *Appl. Phys. Lett.* **109** 253112

[10] English C D, Shine G, Dorgan V E, Saraswat K C and Pop E 2016 *Nano Lett.* **16** 3824–30

[11] Kappera R, Voiry D, Yalcin S E, Branch B, Gupta G, Mohite A D and Chhowalla M 2014 *Nat. Mater.* **13** 1128

[12] Wang L *et al* 2013 *Science* **342** 614–17

[13] SimDM,KimM,YimS,ChoiMJ,ChoiJ,YooSand Jung Y S 2015 *ACS Nano* **9** 12115–23

[14] ShiS,SunZandHuYH2018*J.Mater.Chem.*A **6** 23932–77

[15] Kwak J Y, Hwang J, Calderon B, Alsalman H, Munoz N, Schutter B and Spencer M G 2014 *Nano Lett.* **14** 4511–16

[16] LeongWS,LuoX,LiY,KhooKH,QuekSYandThongJT 2014 *Acs Nano* **9** 869–77

[17] Dahal A and Batzill M 2014 *Nanoscale* **6** 2548–62

[18] Roy T, Tosun M, Kang J S, Sachid A B, Desai S B, Hettick M, Hu C C and Javey A 2014 *ACS Nano* **8** 6259–64

[19] Du Y, Yang L, Zhang J, Liu H, Majumdar K, Kirsch P D and Peide D Y 2014 *IEEE Electron Device Lett.* **35** 599–601

[20] Lin M W, Kravchenko I I, Fowlkes J, Li X, Puretzky A A, Rouleau C M, Geohegan D B and Xiao K 2016 *Nanotechnol.* **27** 165203 [21] Chiappe D *et al* 2018 *Nanotechnol.* **29** 425602

[22] Dumcenco D *et al* 2015 *ACS Nano* **9** 4611–20

[23] Verguts K, Defossez Y, Leonhardt A, De Messemaeker J, Schouteden K, Van Haesendonck C, Huyghebaert C, De Gendt S and Brems S 2018 *ECS J. Solid State Sci. Technol.* **7** M195–M200

[24] Verguts K, Coroa J, Huyghebaert C, De Gendt S and Brems S 2018 *Nanoscale* **10** 5515–21

[25] Liu Y *et al* 2018 *Nature* **557** 696–700

[26] Leonhardt A, Chiappe D, Asselberghs I, Huyghebaert C, Radu I and De Gendt S 2017 *IEEE Electron Device Lett.***38** 1606–9

[27] Cusati T, Fiori G, Gahoi A, Passi V, Lemme M C, Fortunelli A and Iannaccone G 2017 *Sci. Rep.* **7** 1–11

[28] Chanana A and Mahapatra S 2016 *J. Appl. Phys.* **119** 014303

[29] LeeJE,AhnG,ShimJ,LeeYSandRyuS2012*Nat. Commun.* **3** 1–8

[30] ZhuW,LowT,WangH,YePandDuanX2019*2DMater.* **6** 032004

[31] Zhang H, Cao W, Kang J and Banerjee K 2016 Effect of band-tails on the subthreshold performance of 2d tunnel-fets *2016 IEEE Int. Electron Devices Meeting (IEDM)* pp 30–3 IEEE

[32] Kang J, Liu W, Sarkar D, Jena D and Banerjee K 2014 *Phys. Rev.* **4** 031005

[33] LiC,YanX,BaoW,DingS,ZhangDWandZhouP2017 *Appl. Phys. Lett.* **111** 193502

[34] Ortiz-Conde A, S´anchez F G, Liou J J, Cerdeira A, Estrada M and Yue Y 2002 *Microelectronics Reliability* **42** 583–96

[35] Samsudin K, Adamu-Lema F, Brown A, Roy S and Asenov A 2007 *Solid-State Electron.* **51** 611–16

[36] Illarionov Y Y, Rzepa G, Waltl M, Knobloch T, Grill A, Furchi M M, Mueller T and Grasser T 2016 *2D Mater.* **3** 035004

[37] Di Bartolomeo A, Genovese L, Giubileo F, Iemmo L, Luongo G, Foller T and Schleberger M 2017 *2D Mater.* **5** 015014

[38] Yan R H, Ourmazd A and Lee K F 1992 *IEEE Trans. Electron Devices* **39** 1704–10

[39] Liu Y *et al* 2016 *Nano Lett.* **16** 6337–42

[40] Yu L *et al* 2014 *Nano Lett.* **14** 3055–63

[41] Chee S S *et al* 2019 *Adv. Mater.* **31** 1804422

[42] Liu Y *et al* 2015 *Nano Lett.* **15** 3030–4

[43] Cui X *et al* 2015 *Nat. Nanotechnol.* **10** 534

[44] Ling X *et al* 2016 *Adv. Mater.* **28** 2322–9

[45] GuimaraesMH,GaoH,HanY,KangK,XieS,KimCJ, Muller D A, Ralph D C and Park J 2016 *Acs Nano* **10** 6392–9

[46] ZhaoM,YeY,HanY,XiaY,ZhuH,WangS,WangY, Muller D A and Zhang X 2016 *Nat. Nanotechnol.* **11** 954

[47] Huyghebaert C *et al* 2018 2d materials: Roadmap to CMOS integration *2018 IEEE Int. Electron Devices Meeting (IEDM)* IEEE pp 22–1

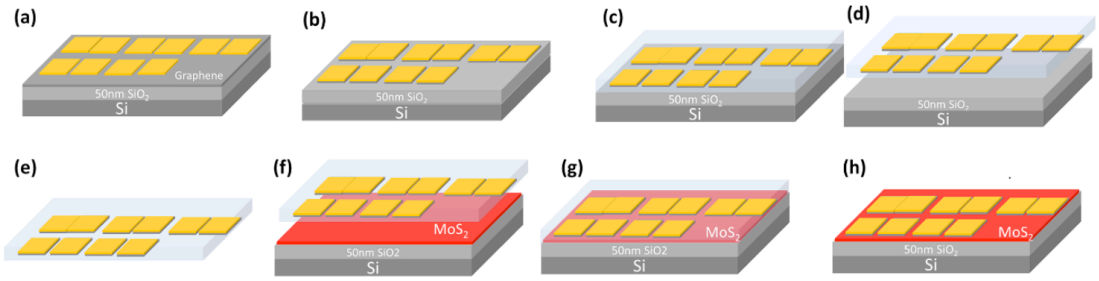

Figure 1. Process flow for the transfer of contacts. (a) Metal contacts are formed on graphene transferred onto a 50 nm SiO_2 substrate with the help of conventional E-beam lithography and metal deposition. (b) Using the metal pads as a mask, the graphene in between is removed using a standard O_2 plasma etch of 1 min. (c) A PMMA layer is then spun on top of the patterned pads and TRT tape is applied gently on top at 80 °C. (d) After water intercalation in DI water for 6 min, the TRT tape is gently peeled away, delaminating the contacts as well. (e) The delaminated stack is dried by blow-drying in N_2. (f) The stack is then aligned onto CVD MoS_2 on 50 nm SiO_2/Si substrate. (g) Both stacks are then stamped together at 80 °C. After stamping, the tape is removed by raising the temperature to 155 °C. (h) PMMA stamp is dissolved in hot acetone (50 °C).

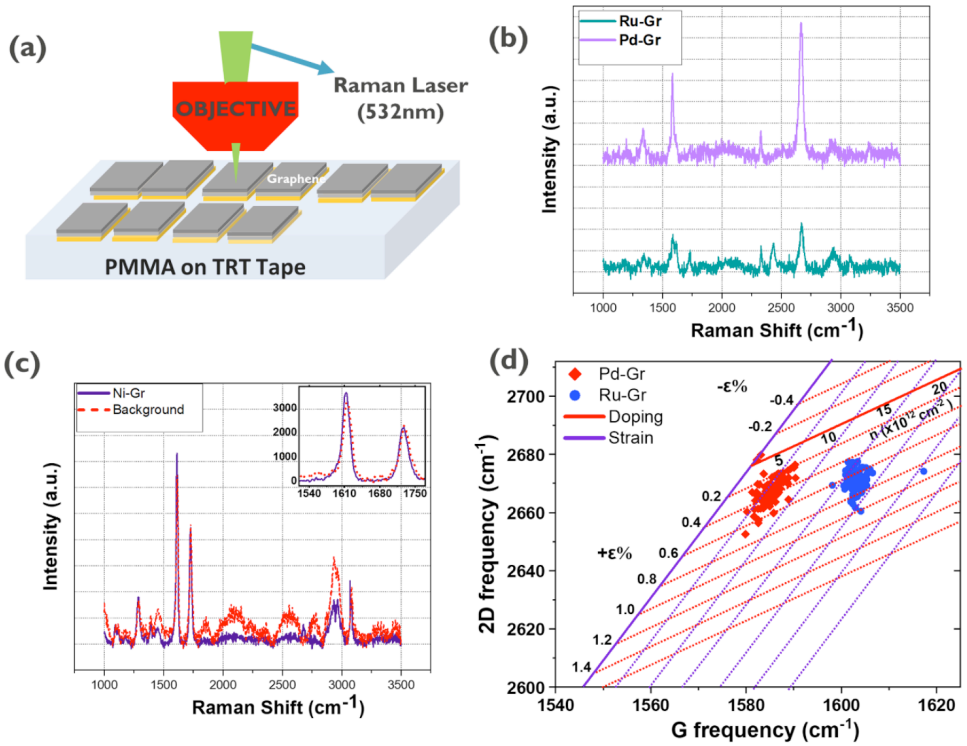

Figure 2. (a) Schematic illustration of the Raman measurement of the metal-graphene stacks. (b) Median Raman spectra obtained from the mappings done on Ru-Gr stack and Pd-Gr stack. Note that the characteristic G and 2D peaks are visible in both cases, substantiating the presence of graphene on the metal contacts. (c) Median Raman spectra obtained from the mappings done on Ni-Gr stack and the spectra obtained from the background. The inset shows that the peaks of Ni-Gr and background match exactly (d) Raman mapping analysis based on the frequency of 2D and G peak. From the figure it can be clearly observed that there is more charge transfer in Ru-Gr than Pd-Gr.

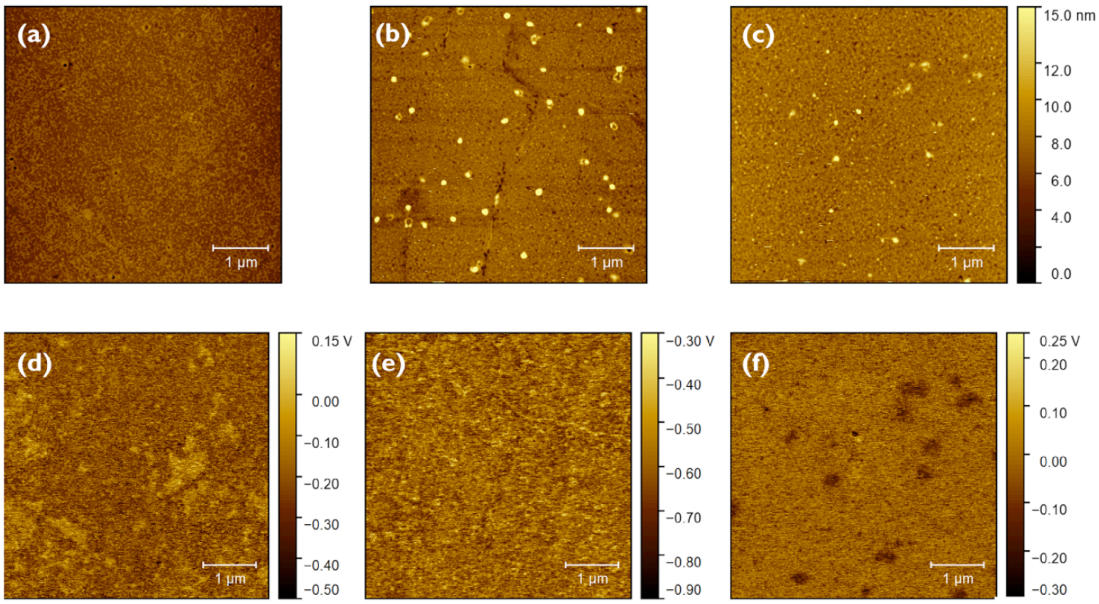

Figure 3. Topography image of the 5 μm $\times$ 5 μm area scanned in the KPFM measurements of (a) Pd-Gr (b) Ru-Gr (c) Ni-Gr. CPD variations across the area measured for (d) Pd-Gr (e) Ru-Gr (f) Ni-Gr.

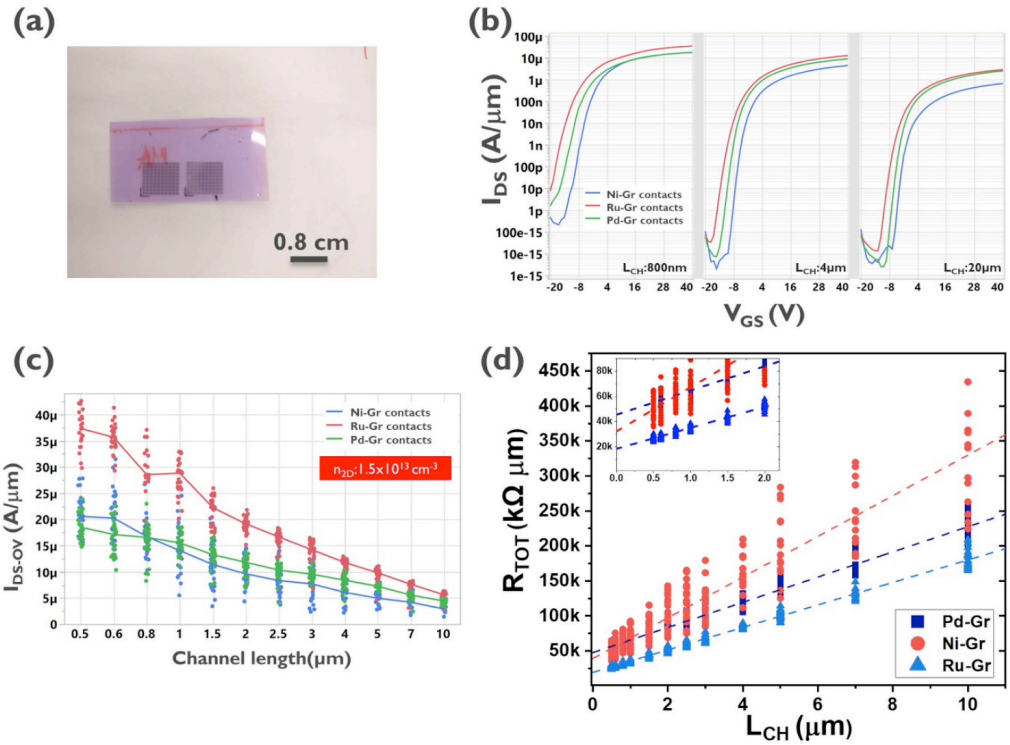

Figure 4. (a) Metal-graphene contact stack TLM sets after being delaminated from the SiO_2 substrate before stamping onto MoS_2 substrate. (b) Median transfer characteristics of Pd-Gr, Ru-Gr and Ni-Gr contacts, measured at $V_{DS} = 1$ V. (c) Source-drain current plotted as a function of channel length for the same gate overdrive voltage corresponding to charge density of 1.5×10^{13} cm^{-2}. The individual points show the current values obtained for a particular channel length and the lines depict the median value trend. (d) Total resistance plotted as a function of channel length for all three metal stacks, at a charge density of 1.5×10^{13} cm^{-2}.

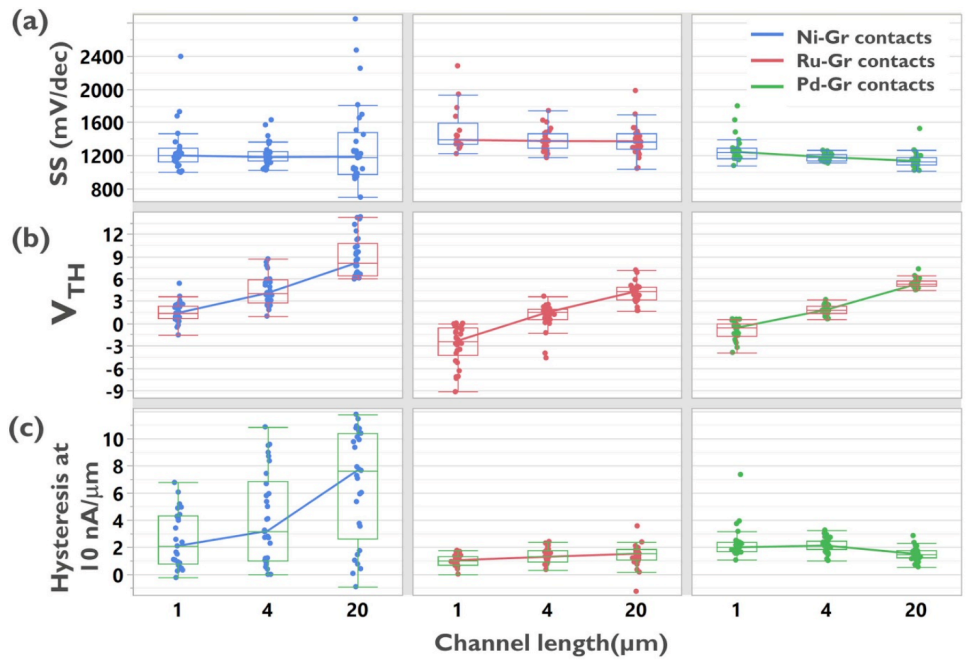

Figure 5. (a) The sub threshold swing of the devices with the three different contact stacks. (b) Threshold voltage trend observed for devices with the three different contact stacks. (c) Hysteresis observed between the forward and reverse sweeps of the devices with the three different contact stacks. The hysteresis value is obtained at a current density value of 10 nA μm^{-1}.

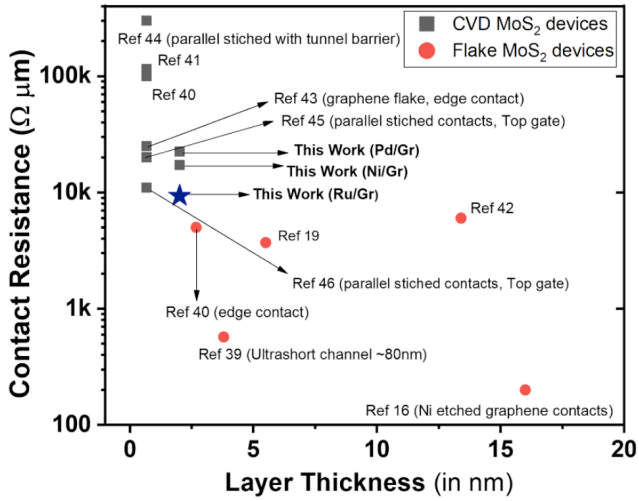

Figure 6. Benchmark plot showcasing the reported contact resistance values [16, 19, 39–46] for graphene contacted MoS_2 devices. The contact resistances are plotted as a function of the MoS_2 layer thickness, for both CVD and flake based devices.